35th Annual International Conference of the IEEE EMBS
Osaka, Japan, 3 - 7 July, 2013

Tubule Detection in Testis Images Using Boundary Weighting and Circular Shortest Path

Chao Zhang[1], Changming Sun[2], Rhonda Davey[3], Ran Su[1], Leanne Bischof[2], Pascal Vallotton[2], David Lovell[4], Shelly Hope[5], Sigrid Lehnert[5], Tuan D. Pham[6]

Abstract— **In studies of germ cell transplantation, measureing tubule diameters and counting cells from different populations using antibodies as markers are very important. Manual measurement of tubule sizes and cell counts is a tedious and sanity grinding work. In this paper, we propose a new boundary weighting based tubule detection method. We first enhance the linear features of the input image and detect the approximate centers of tubules. Next, a boundary weighting transform is applied to the polar transformed image of each tubule region and a circular shortest path is used for the boundary detection. Then, ellipse fitting is carried out for tubule selection and measurement. The algorithm has been tested on a dataset consisting of 20 images, each having about 20 tubules. Experiments show that the detection results of our algorithm are very close to the results obtained manually.**

I. INTRODUCTION

In testis germ cell transplantation, the identification and enrichment of spermatogonial stem cells are two very important steps [2]. Testis weight, scrotal circumference, tubule diameter and numbers of cells of each population are critical to assess testis maturity at different developmental stages [8]. Traditional manual counting methods, which rely on experienced biologists drawing lines and marking cells on tissue images, are tedious and sanity grinding. This paper proposes an automated tubule and cell detection algorithm so that biologists can be relieved from this time consuming work.

One way to detect object boundaries is to use thresholding methods to segment objects based on their brightness. Canny's edge detector [3] detects boundaries or edges by identifying points at which intensities change sharply. The Laplacian of Gaussian (LoG) edge detector can be used to detect closed boundaries. Circular shortest path (CSP) algorithms [7], [11], [12] detect a closed boundary by finding a path on which the pixels have the highest/lowest overall intensities. The ellipse detection method [10] which uses curvature of edges and edge contours as further clues is very effective in detecting ellipses. Active contour methods [9], [5], [4] detect boundaries by minimizing an energy function, requiring that the initial contour be placed close to the boundary. Region growing methods [1], [13] segment objects by comparing one pixel to its neighbors are robust. However, when dealing with tubule detection, region growing will be influenced by the positive cells inside the boundaries.

To overcome the limitations of existing methods, we proposed a new fully automatic tubule detection method based on a boundary weighting transform and the circular shortest paths.

II. TUBULE DETECTION

Our algorithm detects tubule boundaries by first enhancing the linear features of the input image. Then we detect the approximate centers of each tubule region. After that, a window is built at each center point and the window is transformed from Cartesian coordinates to polar coordinates. Then we apply a new boundary weighting transform on the polar transformed image. Next, a CSP is used to detect the boundary and the detected path is transformed back to Cartesian coordinates. Finally, ellipse fitting is used to select tubules perpendicular to the cross section and measurements are made using the parameters of the fitted ellipses.

A. Boundary Enhancement and Center Detection

We first select the image channel in which the tubule boundaries have the highest intensities (Figure 1(b)) and the channel in which the cells have the highest intensities (Figure 1(c)). Then we calculate the difference between the two channels. After that, a morphological image opening operation is carried out to remove noise from the image (Figure 1(d)).

Some parts of tubule boundaries may have strong linear features but not have high intensities compared to neighboring points. Frangi et al. [6] proposed a Hessian matrix based filter to enhance multiscale vessels. In this paper, we add Frangi's filter output (Figure 1(e)) to our image opening result (Figure 1(d)). We see that the contrast between the tubule boundaries and the rest of the image is greatly enhanced.

[1]Chao Zhang and Ran Su are with School of Engineering and Information Technology, The University of New South Wales, Canberra, ACT 2600, Australia and CSIRO Mathematics, Informatics and Statistics, Locked Bag 17, North Ryde, NSW 1670, Australia. kone.zhang@gmail.com, suran.tju@gmail.com

[2]Changming Sun, Leanne Bischof and Pascal Vallotton are with CSIRO Mathematics, Informatics and Statistics, Locked Bag 17, North Ryde, NSW 1670, Australia. changming.sun@csiro.au, leanne.bischof@csiro.au, pascal.vallotton@csiro.au

[3]Rhonda Davey is with CSIRO Animal, Food and Health Sciences, Locked Bag 1, Armidale, NSW 2350, Australia. rhonda.davey@csiro.au

[4]David Lovell is with CSIRO Mathematics, Informatics and Statistics, GPO Box 664, Acton, ACT 2601, Australia. david.lovell@csiro.au

[5]Shelly Hope and Sigrid Lehnert are with CSIRO Animal, Food and Health Sciences, 306 Carmody Road, St. Lucia, Qld 4067, Australia. shelly.hope@csiro.au, sigrid.lehnert@csiro.au

[6]Tuan D. Pham is with Aizu Research Cluster for Medical Engineering and Informatics, Research Center for Advanced Information Science and Technology, The University of Aizu, Fukushima, Japan. tdpham@u-aizu.ac.jp

978-1-4577-0216-7/13/$26.00 ©2013 IEEE

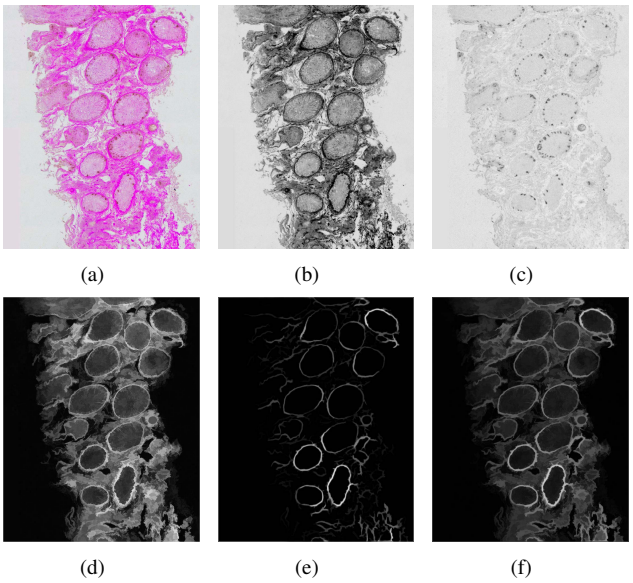

Fig. 1. Boundary enhancement. (a) Original color image. (b) The green channel of the image. (c) The blue channel of the image. (d) The difference between the green channel and the blue channel. (e) Frangi's filter output. (f) The summation of (d) and (e).

Then we need to detect the approximate center of each tubule for the polar transform used in the CSP method. First, an adaptive threshold is used to generate a binary image (Figure 2(a)); second, a dilation is carried out to join discontinuous boundaries and image opening and closing are carried out to remove noise (Figure 2(b)); For each remaining region, an ellipse fitting is carried out and the eccentricity, the short axis, the average distance between the boundary and the fitted ellipse are measured (Figure 2(c)). Since only tubules which are perpendicular to the tissue cross section can reflect the true size of the tubule, regions with a large eccentricity should be removed, and regions that do not fit an ellipse well should also be removed. After the region selection, the average center position of each remaining region is calculated and will be used in the CSP detection part (Figure 2(d)).

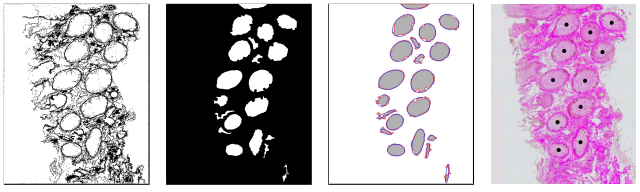

Fig. 2. Illustration of tubule center detection. (a) The result of adaptive thresholding. (b) Dilation of (a). (c) Noise removed using image opening and closing. (d) Detected centers (center points are dilated and overlayed on the original image to better demonstrate the center detection result).

B. Tubule Boundary Detection Using Circular Shortest Path

Once we have estimated the center of each region, the circular shortest path method can be used to detect tubule boundaries. For each center, a window is cropped from the boundary enhanced image (Figure 3(a)). Output of Frangi's filter (Figure 3(b)) is used as a mask so that the program only detects a path within regions where there is a strong linear feature (Figure 3(c)).

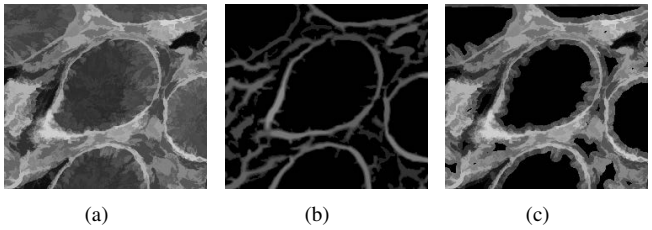

Fig. 3. Window preparation. (a) A window is cropped from the boundary enhanced image. (b) Output of Frangi's filter. (c) Obtaining the region of interest by masking (b) on (a).

To detect the circular shortest path from the image, we first need to polar-transform the input image. Figure 4(a) shows an example of the polar transformed result of Figure 3(c). Problems arise when we use the multiple back-tracking algorithm (MBTA) [11] to detect a shortest path from the image. The red line together with the orange line in Figure 4(b) shows the CSP detection result on Figure 4(a). We see that in some parts of the image, the path does not follow the real boundary (colored by green).

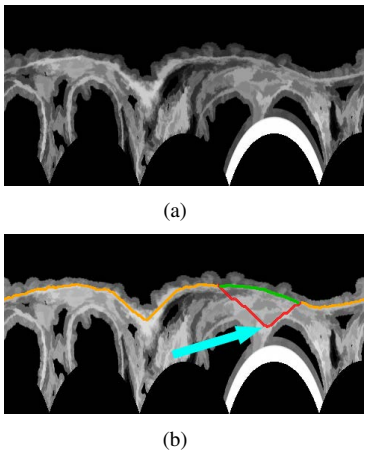

Fig. 4. Polar transform and MBTA detection result. (a) Output of the polar transform. (b) The detected circular shortest path using MBTA.

C. Boundary Weighting Transform

The performance of the circular shortest path method relies heavily on the quality of the input images. In a testis image, the tubule boundaries usually have higher intensities compared with the internal region. However, neighboring tubules also have high intensities, sometimes even higher than those of the current tubule boundary. Since the CSP detects paths on which the overall pixels' intensities is the highest, the detection results may go through another tubule's boundary instead of the current one as we see in Figure 4(b): part of the boundary of the other tubule (indicated by the blue arrow) is much brighter than the current one and therefore the red path has a larger overall intensity values compared with that of the green one.

We propose a new boundary weighting transform to overcome this problem based on the assumption that pixels close to the center should have a larger weighting compared with pixels close to the border. Thus, for each column of the polar transformed image, the weighting should decrease from top to bottom. As pixels of the tubule boundaries are supposed to have higher intensities, in each column the pixels whose intensities are higher than that of its upper and lower pixels can be regarded as a potential boundary point. Then each column can be separated into segments, each of which contains a potential boundary point. The segments are labeled from 1 to n from top to bottom, where n is the number of potential boundary pixels. The segments' weighting decreases from top to bottom while the pixels belonging to the same segment should have the same weighting. Segment i's weighting is calculated by:

$$W_i = w^i$$

where W_i is the weighting of segment number i, and w is the weighting base. In our experiments, we set w to 0.9 based on our test results on 5 random images.

Figure 5(a) shows the output of the boundary weighting of Figure 4(a), (b) is the result of boundary weighting transform and MTBA. We see that now the shortest path follows the tubule boundary precisely.

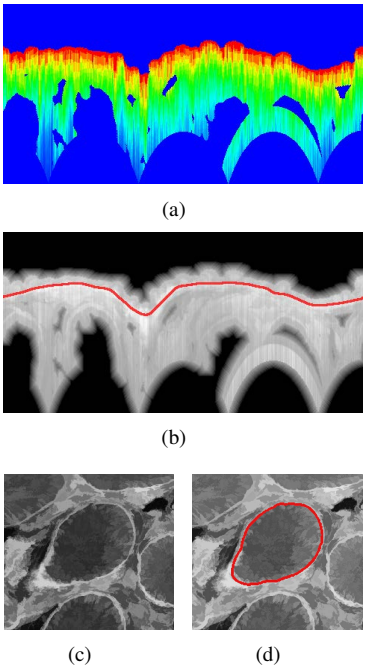

Fig. 5. Boundary weighting on a real image. (a) The output of the weighting function on Figure 4(a). (b) Boundary weighting transform of Figure 4(a) and the result of MBTA CSP. (c) Current window. (d) Transforming (b) back to Cartesian coordinates.

D. Region Selection and Making Measurements

The last step is to fit an ellipse to the detected boundary. We remove regions with eccentricity larger than 1.5, then measure the length of the short axis of the remaining regions. Finally, positive cells within the tubule boundary are detected using adaptive thresholding and split using marker controlled watershed. Figure 6 shows an example of the cell detection result. The white curve shows the detected boundary; the small green objects are detected positive cells.

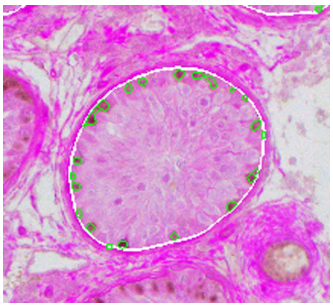

Fig. 6. An example of the cell detection result. Cell boundaries are marked by green curves and tubule boundary is marked by the white curve.

III. EXPERIMENTAL RESULTS

To verify the performance of the proposed method, we tested our algorithm on 20 images using the same parameters. We compare our automated detection results with manually measured and counted results. Figure 7 is part of the detection result of the test image "0-25% 2 min TCT 1380 1103 L GATA4".

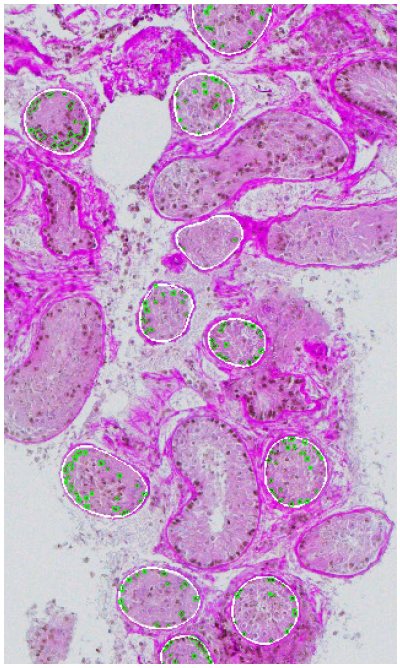

Fig. 7. Part of the detection result on test image: "0-25% 2 min TCT 1380 1103 L GATA4".

Comparison of each tubule's manual count result and automated detection result are shown in Table I. In the table, "TD" is the tubule diameter. We see that the average number of cells the program found is very close to the manual count

result and the average radius of the tubule is also very close to the manually measured size.

TABLE I

COMPARISON OF MANUALLY DETECTION RESULT WITH THE DETECTION RESULT OF THE PROPOSED METHOD OF TEST IMAGE "0-25% 2 MIN TCT 1380 1103 L GATA4".

	Manual count		Automated detection		Difference	
Tubule index	TD (μm)	Cell number	TD (μm)	Cell number	TD (μm)	Cell number
1	134.80	9	133.68	7	1.12	2
2	119.28	7	119.11	8	0.17	1
3	151.99	17	154.07	24	2.08	7
4	138.60	20	116.41	19	22.19	1
5	126.78	15	123.28	17	3.5	2
6	90.44	4	94.71	2	4.27	2
7	98.54	7	98.73	11	0.19	4
8	118.47	5	92.41	14	26.06	9
9	129.58	29	123.12	23	6.46	6
10	120.60	32	121.96	22	1.36	10
12	121.44	12	119.80	14	1.64	2
13	132.02	14	130.07	13	1.95	1
14	116.62	8	108.27	9	8.35	1
16	107.39	19	99.91	19	7.48	0
17	104.08	15	110.60	14	6.52	1
18	110.00	21	115.95	16	5.95	5
20	89.65	21	83.26	15	6.39	6
23	96.21	11	86.75	15	9.46	4
Average	117.03	14.78	112.89	14.55	6.40	3.56

Table II shows the comparison of the manual count result and automated detection result of each image in the dataset. The number in each row is the average radius or cell number of all the tubules in each image. The test results showed that the proposed method is accurate in measuring tubule diameter and detecting positive cells. The program is also used by a biologist on images in a much larger dataset.

TABLE II

COMPARISON OF MANUALLY DETECTION RESULT WITH THE DETECTION RESULT OF THE PROPOSED METHOD ON THE WHOLE DATASET.

	Manual count		Automated detection		Average difference	
Image index	TD (μm)	Cell number	TD (μm)	Cell number	TD (μm)	Cell number
1	117.03	14.78	112.89	14.55	6.40	3.56
2	144.85	21.54	137.67	21.76	4.89	2.76
3	127.65	13.39	120.32	13.71	1.68	2.56
4	151.08	15.59	145.94	13.77	1.74	7.38
5	124.98	13.86	122.04	14.48	2.86	3.60
6	120.86	14.75	120.56	16.41	1.01	4.24
7	116.26	23.89	117.19	25.81	1.23	4.96
8	126.10	20.22	124.46	20.41	1.54	2.05
9	151.36	16.73	136.68	17.15	5.36	2.72
10	139.59	21.10	130.45	22.11	4.75	4.94
11	113.66	14.38	116.96	14.02	3.03	1.46
12	118.54	17.62	114.51	18.75	2.80	3.46
13	132.37	15.41	132.04	16.42	0.84	4.53
14	97.82	22.76	99.63	24.47	1.65	3.97
15	105.12	15.87	94.92	15.00	5.08	3.19
16	151.34	11.64	141.43	11.89	5.28	1.92
17	133.36	18.27	123.22	18.33	2.01	0.74
18	128.36	14.69	122.65	16.35	3.92	6.74
19	119.82	15.42	115.75	13.49	1.66	6.72
20	157.09	13.84	160.00	12.67	2.46	3.99
Average	128.86	16.79	124.46	17.08	3.01	3.77

IV. CONCLUSIONS

Measurements of tubule diameter and numbers of cells of each population are critical for assessment of testis maturity. In this paper a new boundary weighting transform is proposed to provide input for circular shortest path detection. With the new weighting function, circular shortest path can detect accurate boundaries from noisy images. Comparison of the detection results with the manual detection results demonstrates that the performance of measuring tubule diameter and detecting positive cells using the proposed algorithm is very close to that of an experienced biologist.

ACKNOWLEDGMENT

We would like to thank Xiao Tan at CSIRO Mathematics, Informatics and Statistics, Australia, for his helpful comments and discussions. Chao Zhang and Ran Su are partly supported by China Scholarship Council and The University of New South Wales at the Australian Defence Force Academy, Canberra.

REFERENCES

[1] R. Adams and L. Bischof. Seeded region growing. *IEEE Transactions on Pattern Analysis and Machine Intelligence*, 16(6):641–647, June 1994.

[2] U. Borjigin, R. Davey, K. Hutton, and M. Herrid. Expression of promyelocytic leukaemia zinc-finger in ovine testis and its application in evaluating the enrichment efficiency of differential plating. *Reproduction, Fertility and Development*, 22(5):733–742, November 2009.

[3] J. Canny. A computational approach to edge detection. *IEEE Transactions on Pattern Analysis and Machine Intelligence*, 8(6):679–698, November 1986.

[4] V. Caselles, R. Kimmel, and G. Sapiro. Geodesic active contours. *International Journal of Computer Vision*, 22:61–79, 1997.

[5] L. Cohen. Note on active contour models and balloons. *CVGIP: Image Understanding*, 53(2):211–218, March 1991.

[6] A. F. Frangi, W. J. Niessen, K. L. Vincken, and M. A. Viergever. Multiscale vessel enhancement filtering. In *Proceedings of the 1st International Conference on Medical Image Computing and Computer-Assisted Intervention*, volume 1496, pages 130–137, Cambridge MA, USA, 1998.

[7] G. Gallo and S. Pallottino. Shortest path algorithms. *Annals of operations research*, 13:3–79, 1988.

[8] M. Herrid, R. Davey, and J. Hill. Characterization of germ cells from pre-pubertal bull calves in preparation for germ cell transplantation. *Cell and Tissue Research*, 330(2):321–329, November 2007.

[9] M. Kass, A. Witkin, and D. Terzopoulos. Snakes: Active contour models. *International Journal of Computer Vision*, 1(4):321–331, January 1988.

[10] D. K. Prasad, M. K. Leung, and S.-Y. Cho. Edge curvature and convexity based ellipse detection method. *Pattern Recognition*, 45(9):3204–3221, 2012.

[11] C. Sun and S. Pallottino. Circular shortest path in images. *Pattern Recognition*, 36(3):709–719, 2003.

[12] C. Sun, P. Vallotton, D. Wang, J. Lopez, Y. Ng, and D. James. Membrane boundary extraction using circular multiple paths. *Pattern Recognition*, 42(4):523–530, 2009.

[13] S. W. Zucker. Region growing: Childhood and adolescence. *Computer Graphics and Image Processing*, 5(3):382–399, September 1976.